Geophys. J. Int. (1998) **132,** 374–382

On the density distribution within the Earth

B. L. N. Kennett

Research School of Earth Sciences, The Australian National University, Canberra ACT0200, *Australia. E-mail: brian@rses.anu.edu.au*

Accepted 1997 September 7. Received 1997 September 7; in original form 1997 April 18

SUMMARY

The distribution of density as a function of position within the Earth is much less well constrained than the seismic velocities. The primary information comes from the mass and moment of inertia of the Earth and this information alone requires that there be a concentration of mass towards the centre of the globe. Additional information is to be found in the frequencies of the graver normal modes of the Earth which are sensitive to density through self-gravitation effects induced in deformation.

The present generation of density models has been constructed using linearized inversion techniques from earlier models, which ultimately relate back to models developed by Bullen and based in large part on physical arguments. A number of experiments in non-linear inversion have been conducted using the PREM reference model, with fixed velocity and attenuation, but with the density model constrained to lie within fixed bounds on both density and density gradient. A set of models is constructed from a uniform probability density within the bound and slope constraints. Each of the resultant density models is tested against the mass and moment of inertia of the Earth, and for successful models a comparison is made with observed normal mode frequencies. From the misfit properties of the ensemble of models the robustness of the density profile in different portions of the Earth can be assessed, which can help with the design of parametrization for future reference models. In both the lower mantle and the outer core it would be desirable to allow a more flexible representation than the single cubic polynomial employed in PREM.

Key words: density, free oscillations, inversion, reference models.

1 INTRODUCTION

A knowledge of the density distribution within the Earth is important for many aspects of understanding the internal structure of the Earth. In particular, the density is a primary piece of information for unravelling the mineralogical constitution of the Earth; as, for example, in the nature of the temperature gradients in the mantle which influence the balance between the bulk sound speed and the gradient of density with respect to pressure, which forms the basis of the equations used by Williamson & Adams (1923).

The 3-D variation of density is important in relation to the shape of the geoid and the possibility of density variations accompanying the velocity heterogeneity imaged in seismic tomography. However, inferences on 3-D structure are based on linearization about the radial density profile, which by comparison with the seismic wave velocities is not well known.

The agreement between the various models for the Earth's density which have been produced in association with seismic models is high (e.g. Gilbert & Dziewonski 1975; Dziewonski, Hales & Lapwood 1975; Dziewonski & Anderson 1981). However, all these models have ultimately been derived by linearized inversion from models whose origins include a number of physical arguments to supplement the limited range of direct information (see e.g. Bullen 1975 and the references therein).

Apart from sampling at the surface, there is very little possibility of direct observation of density. The major constraints come from the mass and the mean moment of inertia of the Earth about the polar axis, which are moments of the density distribution. The mass is the second moment of the radial density distribution,

$$M = 4\pi \int_0^{r_e} dr r^2 \rho(r), \tag{1}$$

where r_e is the mean radius of the Earth, 6371.0 km. The product of the mass of the Earth and the gravitational constant G is better known than the mass itself; however, a consensus value for the mass is 5.9736×10^{24} kg (Yoder 1995; Cazenave 1995; Dickey 1995). The mean moment of inertia is a scaled fourth moment of the density distribution

$$I = 4\pi \frac{2}{3} \int_0^{r_e} dr r^4 \rho(r) \tag{2}$$

and the currently accepted value in terms of the mass of the Earth is $I = 0.3307144\, Mr_e^2$. Since I is less than would be expected for a uniform body, where the constant of proportionality would be 0.4, there is an immediate requirement for there to be a mass concentration towards the centre of the sphere. The study of Dziewonski & Anderson (1981) leading to the PREM model used a ratio of 0.3308, which is a little larger than the current best estimate. However, Denis *et al.* (1997) have argued that to reconcile the non-hydrostatic ellipticity of internal surfaces it would be appropriate to use a larger ratio, 0.3312, for the effective sphere. Such shifts in the ratio of mass to moment of inertia need to be reflected in adjustments to the radial density distribution.

The main additional source of information on the radial density distribution comes from the free oscillations of the Earth. The frequencies of the spheroidal and radial normal modes are influenced by the density distribution through self-gravitation effects induced during the deformation associated with the mode. The effect is small except for the lowest-frequency modes. The eigenfunctions in radius associated with the different modes provide a range of different samplings of the density structure. The observed frequencies of the normal modes thus provide a means of probing the density structure. However, the interpretation of the free-oscillation frequencies requires a knowledge of the seismic velocity distribution and so the information gained is not wholly independent of other influences.

In this paper we will investigate the level of confidence which can be placed in our knowledge of the density distribution within the Earth by undertaking a set of non-linear inversions using the set of normal mode frequencies published by Masters & Widmer (1995). We will concentrate on different portions of the Earth and work with fixed seismic parameters taken from the PREM model of Dziewonski & Anderson (1981) but allow the density distribution to vary. As a result there will be compensating changes in elastic moduli, but for the cases we have considered, these changes would lie within acceptable limits from mineral physics data.

We specify bounds on both the variation of density and its radial gradient and then use a uniform random sampling procedure within the bounds to produce a sequence of models. Those density models which satisfy the mass and moment-of-inertia constraints are then tested against the free-oscillation frequencies and the misfits in frequency are determined for each mode. The ensemble properties of the set of density models are then used to draw inferences on the character of the radial density distribution.

2 GENERATING AND TESTING DENSITY MODELS

2.1 Data

We have used the set of observed normal mode frequencies prepared by Masters & Widmer (1995), which include estimates of error. From this data set we have extracted the first five radial modes and all spheroidal modes with frequency less than 5 mHz. Direct calculations with and without the effect of self-gravitation indicate that this group of modes collectively shows the most influence of density structure.

The data set is indicated in Fig. 1, in which we display the free-oscillation frequencies calculated from the PREM model (Dziewonski & Anderson 1981) as open symbols and those modes for which there is an observational estimate of frequency as solid symbols. Within this region of the mode table there are still a number of modes with significant density sensitivity for which accurate frequency estimates are not yet available.

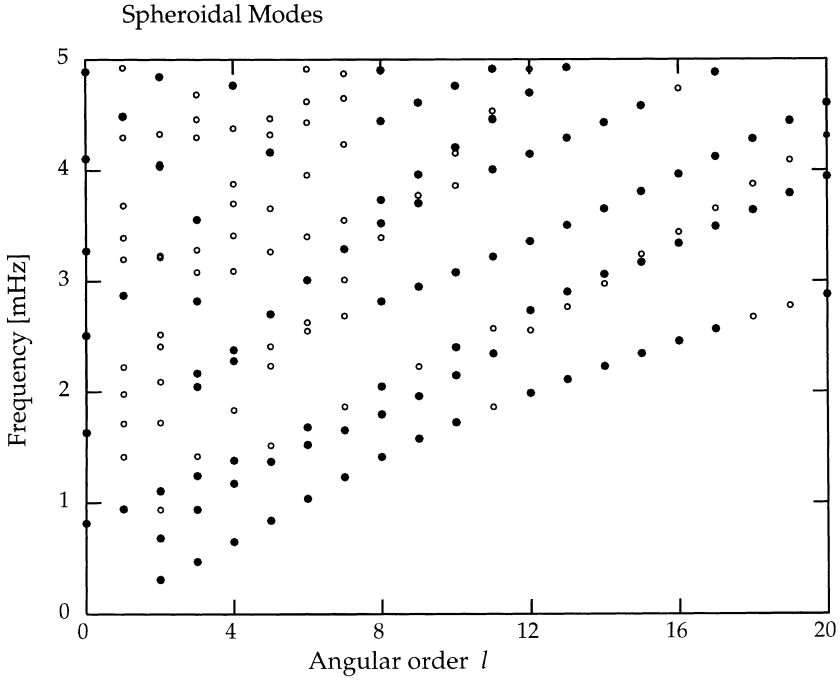

Figure 1. Free-oscillation frequencies for the PREM model as a function of angular order for frequencies less than 5 mHz. Solid symbols mark modes for which observed frequencies are available.

However, recent events, in particular the 1994 deep Bolivian earthquake, have provided a rich new data set from which additional free-oscillation frequencies should be forthcoming (G. Masters, private communication, 1996).

From each postulated density model we construct an earth model by the addition of the PREM values of seismic velocities and attenuation. The free-oscillation frequencies are then calculated afresh for each earth model. No linearization or perturbation approach has been applied. From the calculated normal mode frequencies we prepare a range of misfit criteria, e.g. an L_1 measure formed as the sum of the absolute values of the frequency residuals normalized by the estimated error, or an L_2 measure calculated as the sum of the squares of the normalized frequency residuals. Such measures have been applied independently to the radial modes and to various subsets of the spheroidal modes.

In consequence, for each of an ensemble of putative density models we have a number of misfit criteria which can be used collectively to examine different aspects of the constraints imposed by the available data on the density distribution within the Earth.

2.2 Density model generation

Each of the density models we have tested has been derived by using a uniform random sampling procedure within a set of bounds on density variation and allowed density gradients established around a reference model. The examples presented in this paper are based on the PREM model of Dziewonski & Anderson (1981).

We select a portion of the Earth for specific study and then construct an ensemble of density models for this region using appropriate bounds on the models. We have chosen to specify the density model with a piecewise linear representation in radius. This representation allows rapid calculation of both the mass and the moment of inertia (see Appendix A) but also is convenient for testing the bounds on gradients. A uniform random sampling procedure is used for a specified number of nodes within the bounds at each radius, and the connections between the densities at successive radii have to satisfy the imposed constraints on density gradient. We have used a number of different styles of gradient constraint but have tried to avoid forcing too close a match to the reference model. For example, the most restrictive form employed allowed ± 25 per cent variation from that for the reference model. Various gradient criteria have been used for different regions in the Earth and these will be discussed below. We have not forced any particular smoothness constraints on individual models because we anticipate combining the information from an ensemble of models to provide summary information on the density distribution within a region.

The sampling procedure we have employed gives closer control of the behaviour of the density profile than was available in the pioneering Monte Carlo treatment of Press (1968), which just used constraints on function values and had to employ perturbation techniques to conserve computational resources.

Once a density model has been constructed within the specified bounds, the mass and mean moment of inertia are tested against the reference values and only those models which fit within prescribed tolerances are then compared with free-oscillation data.

For PREM the radial representation used 165 nodes and we have considered density variation in three major regions of the Earth:

(1) the Earth's core (Section 3) from the core–mantle boundary to the centre of the Earth;
(2) the lower mantle (Section 4) from 670 km to the core–mantle boundary with or without forced continuity at 760 km, or at the top of D″;
(3) the upper mantle (Section 5) from the surface down to 800 km with different continuity conditions.

Each sequence of density models was generated from a single random seed and the sampling process was carried out until 100 density models compatible with the mass and moment of inertia were obtained for each seed. We have allowed a tolerance of $\pm 3.25 \times 10^{20}$ kg for the mass and ± 0.0001 for the moment-of-inertia ratio.

The external constraints have proved to have most effect for the models of the lower mantle, for which up to 100 000 random models had to be tested to extract a set of 100 models which could be compared with the free-oscillation data as described above.

2.3 Inference

The patterns of model occupation and misfit were projected onto the bounds about the reference model for each group of 100 models, so that the sampling could be assessed. 500 models were generated for each class of model and from these an attempt was made to extract ensemble properties by ranking models or using different styles of weighted averages to provide varying emphasis on the best-fitting models.

We have found that a suitable means of synthesizing the information content of an ensemble of models is to use distribution functions derived from statistical mechanics. A versatile result is obtainable by using a Boltzmann distribution with an exponential dependence on the misfit function. For this distribution we generate an ensemble property $\langle x \rangle$ by combining information from each of the N models in the ensemble:

$$\langle x \rangle = \frac{\sum_{i=1}^{N} x_i \, \mathrm{e}^{-\beta(E_i - E_0)}}{\sum_{i=1}^{N} \mathrm{e}^{-\beta(E_i - E_0)}}, \tag{3}$$

where x_i is the property associated with the ith model and E_i is the corresponding misfit measure. The reference misfit E_0 would generally be taken as that for the reference model PREM in our case. The quantity β allows the ensemble property to be tuned to vary the influence of different levels of misfit. If β is large, large misfits are heavily downweighted and so the properties are strongly influenced by the best-fitting models. On the other hand, if β is small a broad range of models influence the ensemble properties. In Sections 3–5 we will use the ensemble properties defined through eq. (3) for the density at each depth level $\langle \rho \rangle$ and its variation across the ensemble $\langle (\rho - \langle \rho \rangle)^2 \rangle$.

We have used uniform prior probability for the sampling between the selected bounds subject to the slope constraints. The Boltzmann distribution with a unit value of β then

corresponds to the *a posteriori* likelihood function [*cf.* Sen & Stoffa (1995), Chapter 7].

A stronger selectivity for those models in the ensemble with the smallest misfits can be produced by replacing the exponential Boltzmann distribution of eq. (3) with a Bose–Einstein distribution,

$$\frac{1}{e^{\beta(E_i - E_0)} - 1}, \tag{4}$$

in which case the choice of reference misfit E_0 needs to be made with some care since eq. (4) becomes singular as E_i approaches E_0. For large misfit eq. (4) approaches an exponential.

3 THE EARTH'S CORE

We will first consider allowing the density structure to vary from that for PREM over the region from the core–mantle boundary to the centre of the Earth. In the PREM reference model the density in the core is represented by a cubic in radius from the core–mantle boundary down to the inner-core boundary and by a quadratic in the inner core. We have imposed density bounds at $\pm 40\,\mathrm{kg\,m^{-3}}$ from the PREM values and have considered a number of different constraints on the radial gradient of density. The density is allowed to vary at 66 depth levels with nodes $6.66\,\mathrm{kg\,m^{-3}}$ apart. With the piecewise linear density models we have a potential sample space of some 10^{34} models and as a result no sampling procedure can be expected to explore all possibilities. However, we tried to broaden the range of models considered in a limited sample by starting each group of models from a different random seed and then combining a number of different groups into an ensemble.

For the Earth's core, although the densities are quite high, the mass and moment of inertia associated with any shell are relatively small and the requirement of matching the mass and mean moment of inertia within the prescribed tolerance imposes little structure other than that in PREM itself. Only a few models were rejected for each random seed from the primary contraints.

We have considered three different sets of assumptions about the nature of the velocity gradients in the core and the discontinuity at the inner-core boundary. In the first trial we used weak bounds on gradients (from −25 to 125 per cent of the gradient at that level in PREM) but imposed a requirement of an increase in density at the inner core. The second trial allowed either a decrease or an increase of density at the inner-core boundary with the same slope constraints. In the third trial we narrowed the gradient bounds to the range 25 to 125 per cent of the PREM value with no constraint on the jump at the inner core. Very similar results are obtained in all three cases.

The piecewise linear models do not have any intrinsic smoothness requirement and from each random seed a significant number of models can be generated which achieve a lower misfit to the observed free-oscillation frequencies than the reference model PREM. The parametrization is designed to allow the reference model to be acceptable but it must be recognized that this is a low-probability event. In Fig. 2 we display the L_1 and L_2 measures of misfit relative to the PREM value as a function of model number, ranked by the size of misfit. The general level of fit is very good but there are about 50 models which are significantly better than the rest. The shape of the misfit patterns as a function of ranked model is characteristic of most of the cases we have considered; there are a few models with small misfits and a few with poor performance and a smooth progression between. However, the scaling of the misfits varies between different segments of the Earth.

An informative way of looking at the results of the model generation process is to look at the pattern of models as a function of depth and at the way in which the misfit maps into the density distributions. This is illustrated in Fig. 3, where we display 100 models generated from a single random seed in the third trial. In the left-hand panel of Fig. 3, the models are displayed relative to the PREM values and the density of the

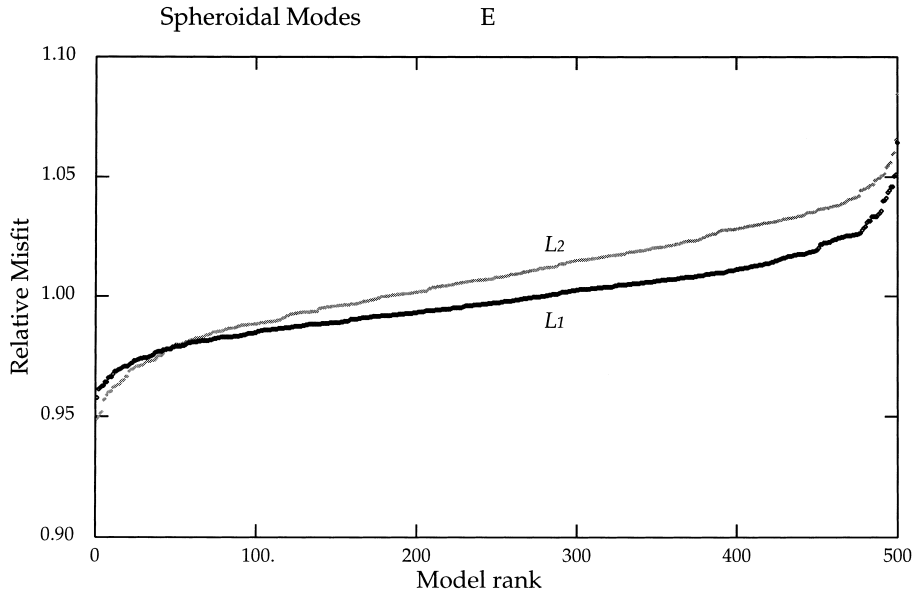

Figure 2. Display of L_1 and L_2 misfit measures relative to the PREM reference for 500 core models in rank order.

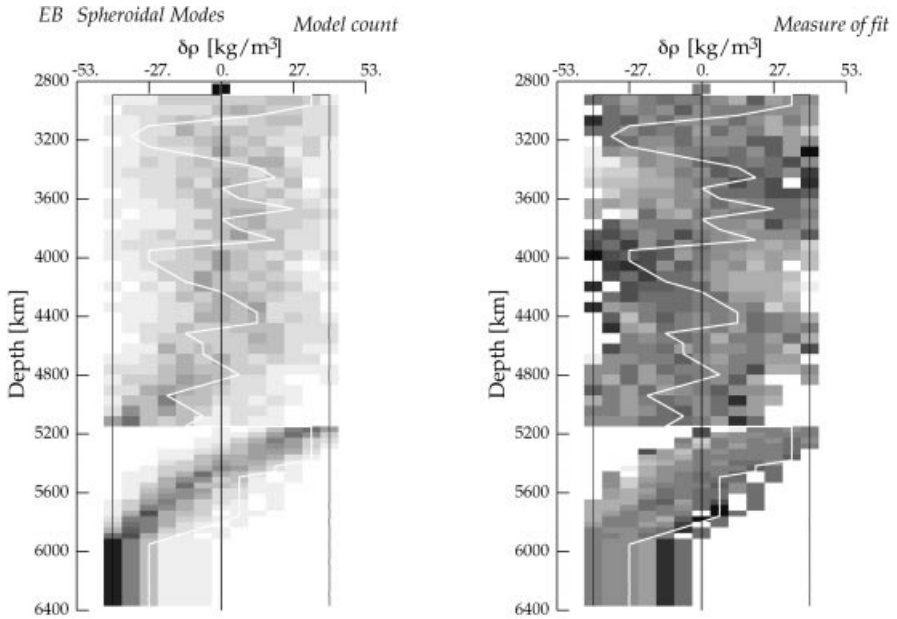

Figure 3. Display of sampling and projected model misfit for a set of 100 models of density structure in the core derived from the same random seed. The model with the least L_2 misfit is superimposed in white.

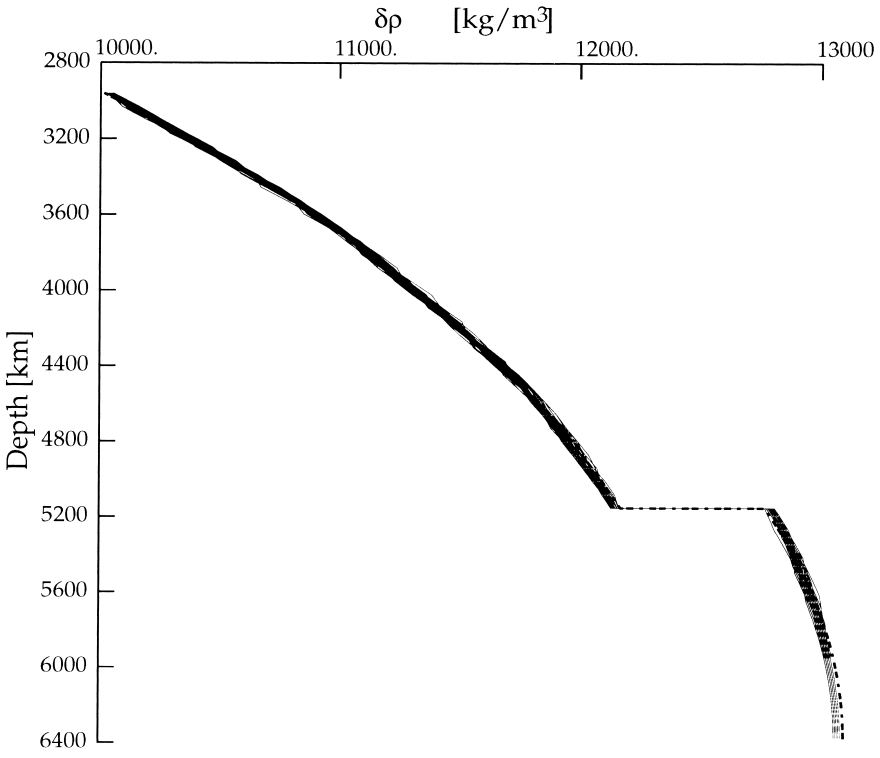

Figure 4. The 50 density models for the core region with the least L_1 misfit, compared to PREM reference model shown as a chain-dashed line.

grey shade represents the model count in each cell; superimposed in white is the best-fitting model using an L_2 norm criterion. A broad sampling of the allowed density bounds has been achieved in the outer core, but a more concentrated pattern emerges in the inner core, which arises from the broad range of allowed gradients. In the right-hand panel of Fig. 3 we project the misfit onto the model space by representing the mean misfit per cell for each model that passes through that region. We note immediately that the best fits can appear at the fringes of the sampled zone.

The deviations in both slope and density value from the reference model are not large and are somewhat exaggerated by the presentation in Fig. 3. In Fig. 4 we have therefore displayed the best 50 models from the L_1 misfit criterion, with the PREM model superimposed as a chain-dashed line. The most noticeable feature is the trend to lower densities and gradients in the inner core, which helps to improve the fit to the free-oscillation information.

The gradients in the PREM model lie very close to adiabatic stratification (the Adams–Williamson condition). We have allowed significant departures from this behaviour in order to provide a sampling of a broad region around the reference model. The imposition of tighter slope bounds tends to restrict the zone of acceptable models but has to be used judiciously to avoid artificial restrictions on connectivity between successive levels in the model.

So far we have considered the models in isolation, but we can reimpose some degree of smoothness by looking at the ensemble properties. In Fig. 5 we display a comparison of two sets of ensemble estimates. The grey lines are for a small value of β so that the full range of 500 models in the ensemble will contribute. The chain-dotted lines indicate the estimate of the variance associated with this estimate. The solid lines are for a fourfold increase in β so that the emphasis is on the best-fitting models; as a result the combination is somewhat rougher. In each case the jump at the inner-core boundary is enhanced.

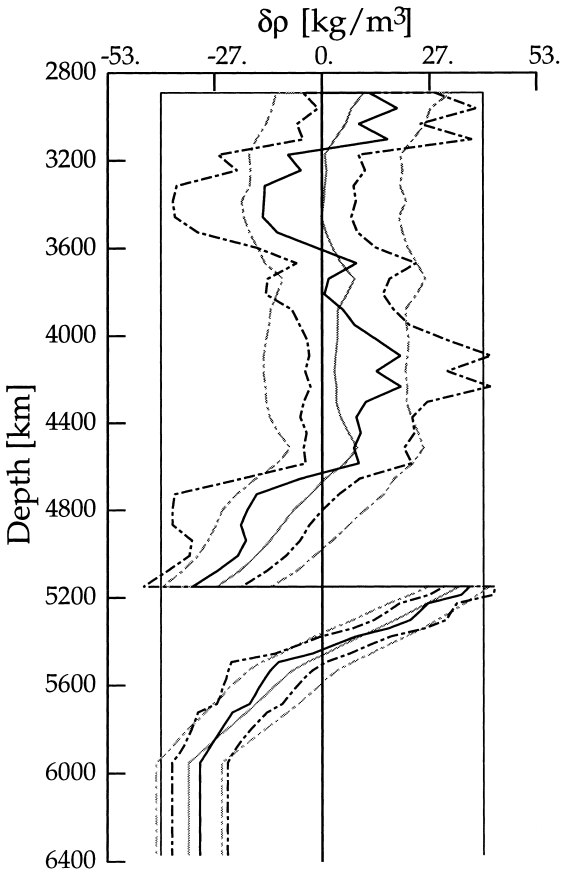

Figure 5. Ensemble average structures for density and its variation in the core, using an exponential weighting with misfit. The grey lines represent the case where a broad range of models is included; the black lines are for a choice of β to emphasize the best-fitting models.

The ensemble results suggest that in the outer core down to 4400 km a simple cubic in radius is adequate. But, in the parametrization of density in the core it would be advantageous to allow a separate representation of the zones on the two sides of the inner-core boundary rather than force a single low-order polynomial in each of the inner and outer cores.

Alternatively, a higher-order Chebyshev polynomial could be used in the outer core to provide a flexible representation without undue instability.

4 THE LOWER MANTLE

We now retain the PREM structure in the core and look at the possible variation of density in the lower mantle, which we have taken as the region from 670 km deep to the core–mantle boundary. This zone is represented in the PREM model with a cubic polynomial in radius from 670 km to 771 km depth, a cubic polynomial from 771 km to 2741 km at the top of D″, and a further cubic to the core–mantle boundary; continuity of density is imposed at 771 km and 2741 km depth. We have used a rather different representation, with a set of linear gradients in radius, and in consequence we can test the appropriateness of the PREM parametrization.

Once a discontinuity is allowed, the probability is overwhelmingly in favour of it developing some contrast, and so if just a discontinuity in gradient is expected it is necesary to impose continuity in the density itself. Thus, at 771 km depth we have normally imposed a continuity condition. However, at the top of D″ we have considered cases in which we have forced continuity and also where we have allowed a discontinuity to develop.

We have imposed density bounds at ± 40 kg m^{-3} from the PREM values, with nodes 5.0 kg m^{-3} apart for 63 depth levels, which gives a sample population of around 10^{25} potential models.

For this lower-mantle section, we have found that the mass and moment-of-inertia constraints are of major importance, and that for a single random seed between 30 000 and 150 000 models would need to be generated to produce 100 which satisfied the primary constraints within our prescribed tolerances and which then could be compared with the free-oscillation information.

The mass and moment-of-inertia constraints, when applied to this segment of the Earth, have led to a characteristic banding in the model sampling, which is well illustrated in the left-hand panel of Fig. 6, which follows the same format as Fig. 3. A set of 100 models derived from a single random seed is displayed to illustrate the patterns of model sampling (nearly 60 000 models were rejected on the basis of the primary constraints) and misfit. The best-fitting models tend to have somewhat lower density gradients than the general trend of the cluster. For the lower mantle it was difficult to find models that fitted as well as PREM unless a discontinuity was allowed at the top of D″. The overall span of misfits was somewhat larger than in the core, with misfit measures reaching about 1.3 times the PREM values.

In Fig. 7 we display the ensemble estimates for the density distribution and its variation in the lower mantle. When a

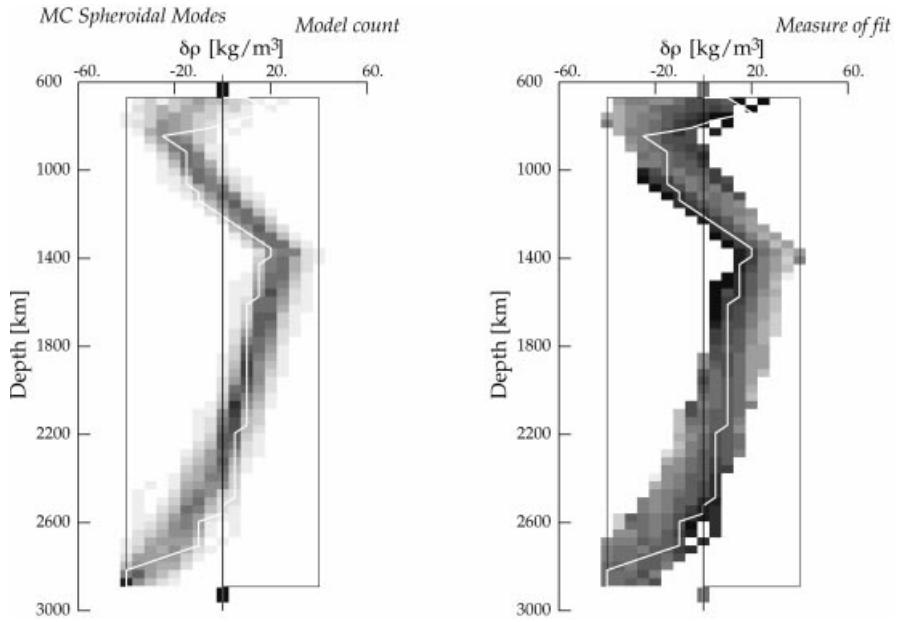

Figure 6. Display of sampling and projected model misfit for a set of 100 models of density structure in the lower mantle derived from the same random seed. The model with the least L_2 misfit is superimposed in white.

broad span of models is allowed (grey lines), the behaviour follows closely the trend seen in the model sampling in Fig. 6. However, when attention is focused on the models with a better fit to the free-oscillation data (black lines) there is a reduced gradient between 1400 and 2600 km depth, with a mean departure of 0.016 kg m^{-3} from PREM so that effectively the Williamson–Adams condition for an adiabatic temperature is sustained. We note in Fig. 7 that the better models develop a very clear transition into D″, even though no discontinuity was allowed in this set of trials.

When discontinuities were allowed at 771 km and 2741 km, relatively minor jumps developed at 771 km but large jumps were common at 2741 km. Away from the immediate vicinity of the discontinuities the behaviour was very close to that illustrated in Figs 6 and 7.

We can expect there to be some edge effects associated with the isolation of only a portion of the Earth, but the patterns of behaviour in Figs 6 and 7 suggest that it would be desirable to allow at least two cubic polynomial segments in any future parametrization of the density distribution in the lower mantle.

5 THE UPPER MANTLE

In this case we have retained the PREM structure for depths below 800 km but have allowed the density to vary through the upper mantle and have looked at a range of different continuity conditions.

The PREM parametrization in the upper mantle is in terms of linear gradient segments, so that there is a closer correspondence with the model representation in this region than for the two deeper zones. We have allowed density variation of up to ± 100 kg m^{-3} from the PREM values, with nodes 5.0 kg m^{-3} apart at 40 depth levels. The size of the sample population varies somewhat with different continuity conditions, but is not less than 10^{27} potential models. The influence of the mass and moment-of-inertia constraints is relatively weak for this portion of the Earth because only a small portion of the mass is involved and the conditions can be fitted by adjustment of density between different levels.

The deviations in density which we have allowed in the upper mantle extend well outside any plausible linearization conditions. The span of the misfits over the 500 model ensemble for each class of trial is substantially larger than for the other cases but a few models approach the fit achieved with PREM or even improve on it.

In these cases we have found it most effective to use the Bose–Einstein representation (eq. 4) for the ensemble properties because of its emphasis on the models with the least misfit to the free-oscillation frequencies. As shown in Fig. 8 for the L_1 misfit measure, the ensemble properties favour a slight increase in the density contrast at the 210 and 400 km discontinuities and a slight decrease in the contrast 670 km. The estimated variance is significant and is reflected in the behaviour of the 50 best models on the L_1 criterion, which are illustrated in Fig. 9.

The level of misfit can be reduced by the introduction of further discontinuities so that in this depth range the prior specification of potential jumps in density is important. For example, the PREM model includes a discontinuity at 210 km which is of major significance for velocity, yet the presence of such a global feature is certainly a matter of dispute.

6 DISCUSSION AND CONCLUSIONS

The sequence of model tests described in this paper has been undertaken to try to get an assessment of the constraints available on the density distribution without invoking linearization about a reference model. The representation of the models has been deliberately chosen to differ significantly from the PREM model with which comparisons have been

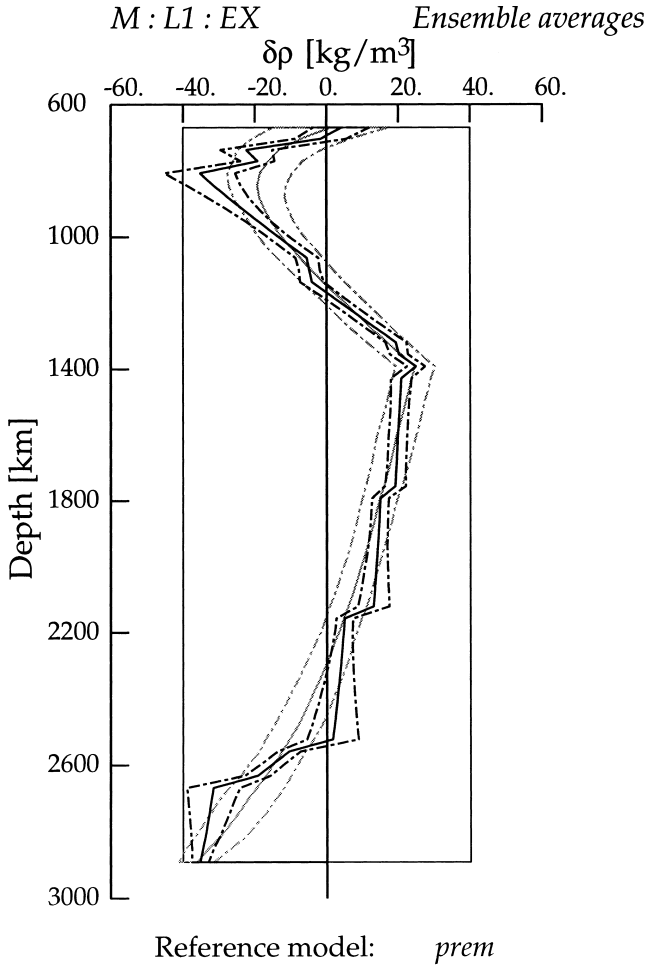

Figure 7. Ensemble average structures for density and its variation in the lower mantle using an exponentional weighting with misfit. The grey lines represent the case where a broad range of models is included; the black lines are for a choice of β to emphasize the best-fitting models.

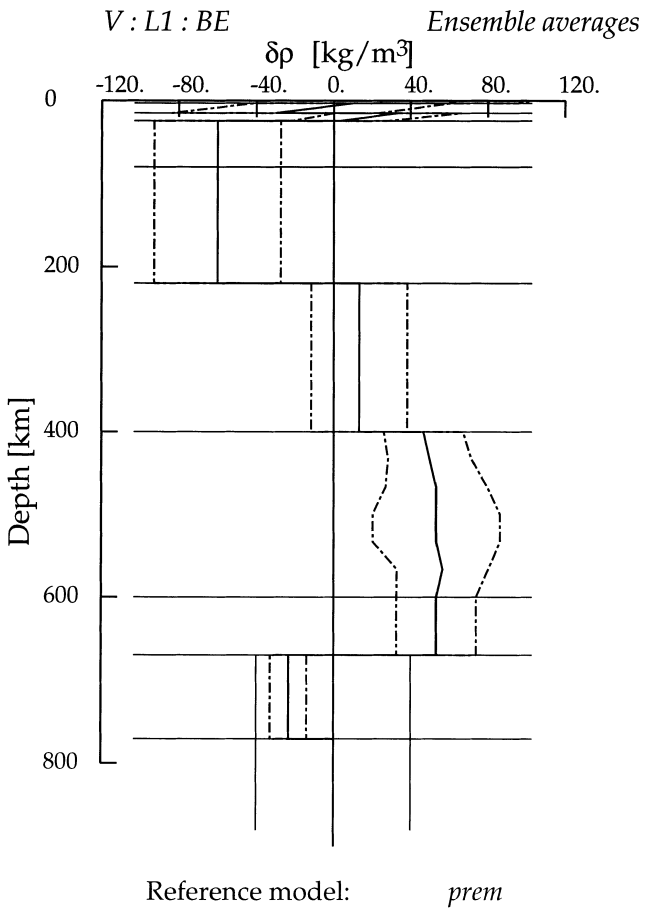

Figure 8. Ensemble average structures for density and its variation in the upper mantle using a Bose–Einstein weighting which emphasizes the properties of the best-fitting models.

made, so that an assessment can be made of the adequacy of the polynomial parametrization employed in PREM. In addition to employing results from groups of models derived from a single random seed, we have used ranked model information across an ensemble of 500 models. We have also looked at ensemble properties for density and its variance as a function of depth, using both an exponential and a Bose–Einstein weighting in terms of individual model misfit. The ensemble properties allow the reinstatement of smoothness, which is missing in the individual piecewise linear representations.

The many trials demonstrate the quality of the PREM density model, particularly as a smooth model within the limits of its parametrization. However, the constraints imposed on the polynomials for the different depth intervals in PREM are based on mathematical convenience rather than an attempt to allow for different physical processes.

For both the lower mantle and the core, it would be desirable for any future reference models to have more degrees of freedom than in PREM. A single cubic polynomial in radius is barely adequate to represent the full range of behaviour across a major zone within the Earth, and imposes a very strong constraint on the nature of possible gradients. In particular, it is desirable that special provision is made for the treatment of structure near major boundaries.

In future representations of the spherically averaged density models, we must be wary of forcing excessively heavy constraints on our view of the Earth by working with a very limited number of parameters, which is no longer required with recent advances in computational power.

The details of the density models would be modified if we adopted a dynamic density model with a modified moment of inertia, rather than the hydrostatic case as considered above, but this would not affect our conclusions.

ACKNOWLEDGMENTS

I would like to thank Guy Masters for the version of the MINOS program used in calculating the free-oscillation frequencies used in this work and for general discussions. I would also like to thank Malcolm Sambridge, who created the original routines for uniform sampling with function and gradient bounds and who has been very helpful in discussions on extraction of model properties from ensembles. Malcolm Kennett helped with the development of the inversion scheme.

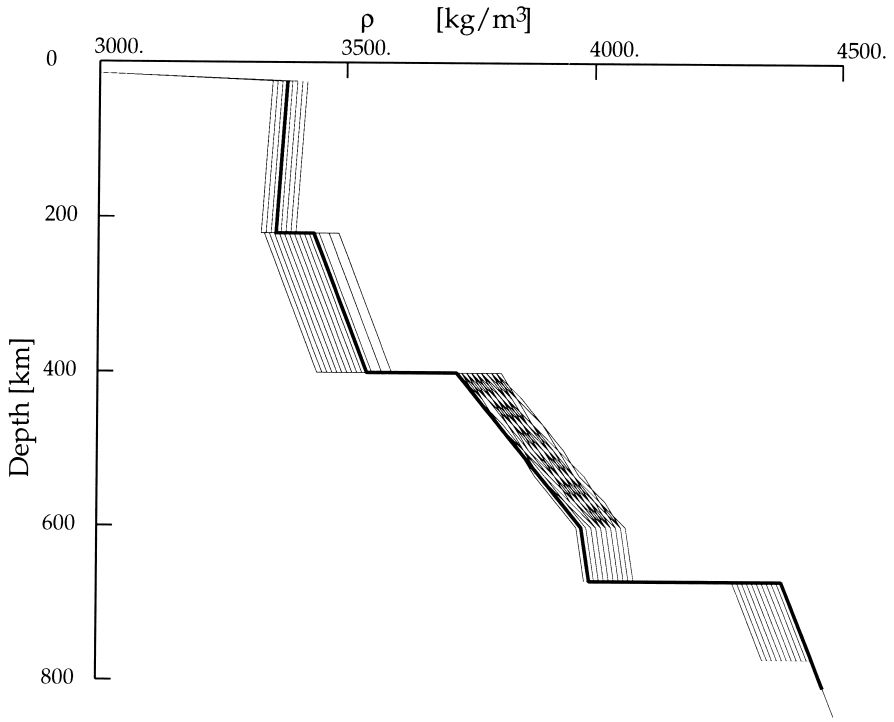

Figure 9. The 50 density models for the upper mantle region with the least L_1 misfit, compared to the PREM reference model shown as a heavy black line.

REFERENCES

Bullen, K.E., 1975. *The Earth's Density,* Chapman & Hall, London.

Cazenave, A., 1995. Geoid, topography and distribution of landforms, in *Global Earth Physics: a Handbook of Physical Constants,* pp. 32–39, ed. Ahrens, T.J., American Geophysical Union, Washington, DC.

Denis, C., Rogister, Y., Amalvict, M., Delire, C., Denis, A.Í. & Munhoven, G., 1997. Hydrostatic flattening core structure, and the translational mode of the inner core, *Phys. Earth planet. Inter.,* **99,** 195–206.

Dickey, J.O., 1995. Earth rotation, in *Global Earth Physics: a Handbook of Physical Constants,* pp, 356–363, ed. Ahrens, T.J., American Geophysical Union, Washington, DC.

Dziewonski, A.M. & Anderson, D.L., 1981. Preliminary reference Earth model, *Phys. Earth planet. Inter.,* **25,** 297–356.

Dziewonski, A.M., Hales, A.L. & Lapwood, E.R., 1975. Parametrically simple Earth models consistent with geophysical data, *Phys. Earth planet. Inter.,* **10,** 12–48.

Gilbert, F. & Dziewonski, A.M., 1975. An application of normal mode theory to the retrieval of structural parameters and source mechanisms from seismic spectra, *Phil. Trans. R. Soc. Lond.,* A, **278,** 187–269.

Masters, T.G. & Widmer, R., 1995. Free oscillations: frequencies and attenuation, in *Global Earth Physics: a Handbook of Physical Constant,* pp. 104–125, ed. Ahrens, T.J., American Geophysical Union, Washington, DC.

Press, F., 1968. Earth models obtained by Monte-Carlo inversion, *J. geophys. Res.,* **73,** 5223–5234.

Sen, M. & Stoffa, P.L., 1995. *Global Optimization Methods in Geophysical Inversion,* Elsevier, Amsterdam.

Williamson, E.D. & Adams, L.H., 1923. Density distribution in the Earth, *J. Wash. Acad. Sci.,* **13,** 413–428.

Yoder, C.F., 1995. Astrometric and geodetic properties of the earth and the solar system, in *Global Earth Physics: a Handbook of Physical Constants,* pp. 1–31, ed. Ahrens, T.J., American Geophysical Union, Washington, DC.

APPENDIX A: DENSITY MODELS

We work with density models specified as a sequence of values $\rho(z)$ at successive depth points $z = r_e - r$, where the radius of the Earth $r_e = 6371$ km. A linear interpolation is used between grid points with allowance for possible discontinuities, in terms of normalized radius:

$$\rho(r) = a_i + b_i(r/r_e), \quad q_i < r < q_{i+1},$$
$$= \rho(q_i) + b_i(r - q_i)/r_e.$$

In this formulation the mass is given by

$$\frac{M}{4\pi r_e^3} = \sum_{i=0}^{N-1} \left\{ \left(\frac{q_{i+1}}{r_e}\right)^3 \left(\frac{a_i}{3} + \frac{b_i}{4}\frac{q_{i+1}}{r_e}\right) - \left(\frac{q_i}{r_e}\right)^3 \left(\frac{a_i}{3} + \frac{b_i}{4}\frac{q_i}{r_e}\right) \right\}$$

and the mean moment of inertia by

$$\frac{I}{4\pi r_e^5} = \sum_{i=0}^{N-1} \left\{ \left(\frac{q_{i+1}}{r_e}\right)^5 \left(\frac{a_i}{5} + \frac{b_i}{6}\frac{q_{i+1}}{r_e}\right) - \left(\frac{q_i}{r_e}\right)^3 \left(\frac{a_i}{5} + \frac{b_i}{6}\frac{q_i}{r_e}\right) \right\}.$$